Preprints of the 21st IFAC World Congress (Virtual)
Berlin, Germany, July 12-17, 2020

Friction Compensation and Limit Cycle Suppression at Low Velocities Based on Extended State Observer

Minnan Piao * **Ying Wang** ** **Mingwei Sun** * **Zengqiang Chen** *

* *College of Artificial Intelligence, Nankai University, China (e-mail: smw_sunmingwei@163.com).*
** *Science and Technology on Space Physics Laboratory, China*

Abstract: This paper investigates the extended state observer (ESO) based friction compensation at low velocities with only the position measurement. ESO is an effective model-free friction compensation technique and thus is employed in this paper. Based on the describing function analysis, it is revealed that the higher the observer bandwidth is, the larger the velocity feedback gain should be to suppress the limit cycle. However, the available damping provided by the derivative control is restricted when the signal-to-noise ratio of the velocity is low. Under such a condition, the observer bandwidth cannot be high and the friction compensation performance is thus limited. To solve this conflict, a switching control law based on the ESO is proposed to compensate the friction in a fast manner and suppress the limit cycle simultaneously. The switching strategy aims to determine when the disturbance compensation should be added in the control signal to eliminate the friction induced oscillations without making the system response become sluggish. Such an idea is enlightened by the fact that nonlinear modifications to the integral action are always needed in practice. Hardware experiments are performed on a brushless DC motor to validate the effectiveness of the proposed compensation scheme.

Keywords: Friction compensation; Low velocities; Extended state observer; Limit cycle; Switching strategy

1. INTRODUCTION

When mechanical systems execute the positioning or low-velocity tracking tasks, the effect of friction is dominant and is the main cause of performance degradation. Therefore, the friction compensation at low velocities is critical to achieve high-precision position control.

Much effort has been devoted to the friction compensation. Armstrong et al. (1994) performed a thorough and detailed survey about the compensation methods. In general, the investigations can be classified into two categories: the friction-model based compensation (FMC) and the non-friction-model based compensation (NFMC). In the FMC framework, a parametric friction model with fixed or adaptive parameters should be established first (Garagić and Srinivasan (2004); Huang and Tan (2012); Xia et al. (2013)). Since the friction models are all dependent on the velocity, the quality of the velocity signal is significant especially for the low-velocity scenario wherein the signal-to-noise ratio (SNR) is relatively low (Armstrong et al. (1994)). Although the command velocity can be used instead for the low velocities, the approximation error may degrade the compensation performance greatly. Thus, the NFMC scheme is more favorable when the quality of the velocity signal is not good enough.

Within the NFMC framework, the high-gain proportional-derivative (PD) control is the most popular approach that has been used in industry. The tracking error can be reduced by designing high feedback gains, while the measurement noise will be amplified and the robustness to the high-frequency unmodeled dynamics (like the flexible dynamics) will be deteriorated in this way. When the PD control cannot realize the desired precision, the integral action is almost always introduced. By using the accumulative effect of the error, the need for the high PD gains can be alleviated. However, the undesirable limit cycle may be generated and the integral windup tends to happen when there is a velocity reversal. Armstrong et al. (1994) summarized many modification methods of the integral control based on the practical experiences of engineers. With the development of the uncertainty and disturbance estimation and attenuation (DUEA) technique (Chen et al. (2016)), the disturbance observer has become a popular approach in the NFMC scheme (Lee and Tomizuka (1996); Friedland and Park (1997); Ishikawa and Tomizuka (1998); Jamaludin et al. (2009); Huang et al. (2009); Ahmed-Ali et al. (2009); Sun et al. (2013); Wang et al. (2016); Ren et al. (2019)). The disturbance observer can be combined with a fixed friction model to tackle the unmodeled friction (Lee and Tomizuka (1996); Jamaludin et al. (2009)) or employed to estimate the friction without any model information (Sun et al. (2013); Wang et al. (2016)). An extended state observer (ESO) (Han (2009); Gao (2003)) was employed by Sun et al.

⋆ This work was supported by National Natural Science Foundation of China under Grant 61573197, 61973175, and 51777013.

(2013) to attenuate the aftereffect of the friction on the output of a traditional PD control system. The ESO was first proposed by Han (2009) in his effort to develop an alternative approach, active disturbance rejection control (ADRC), to the classic PID control. Different from other disturbance observers, only the relative degree and the control gain are required for the ESO design. All the internal uncertainties and external disturbances that affect the controlled output can be regarded as an extended state and estimated by the ESO. As can be seen from the equivalent form of the control law based on the ESO, there exists the integral effect and the limit cycle may be generated in the presence of the Coulomb and static frictions (Armstrong and Amin (1996)). When the SNR of the velocity is very low, the feedback gain of the velocity is restricted and the limit cycle suppression can only be achieved by reducing the observer bandwidth. However, the friction compensation performance will be degraded by a low observer bandwidth. Consequently, how to solve the conflict between the friction compensation and limit cycle is critical when employing the ESO under such a scenario. Although many applications of the ESO on the friction compensation have been done (Wang et al. (2016); Ren et al. (2019)), the effect of the disturbance observer on the limit cycle has been rarely investigated.

Motivated by the analysis above, an ESO based NFMC approach is proposed for the friction compensation and limit cycle suppression at low velocities. A brushless DC motor (BLDCM) is selected as the benchmark. The effects of the control and observer gains on the limit cycle are investigated based on the describing function and the restriction of parameter tuning is revealed. Enlightened by the fact that nonlinear modifications to the integral action in the PID control are necessary, a switching strategy is established in this paper to eliminate the limit cycle without making the system response become sluggish. The switching signal is designed as the function of the tracking error and the command velocity to determine when the disturbance compensation should be added in the control signal. The relationship between the command velocity and the limit cycle is obtained through the experiment to derive the critical velocity threshold used in the switching strategy. Hardware experiments are carried out to validate the effectiveness of the proposed method.

The remainder of the paper is organized as follows. The mathematical model of the BLDCM is shown in Section 2. The ESO based switching control strategy is proposed in Section 3. Section 4 presents the effects of the parameters on the limit cycle and the restriction of parameter tuning. The experiment results are provided in Section 5. Finally, concluding remarks are given in Section 6.

2. MODEL DESCRIPTION

In this study, the BLDCM is used. The simplified mathematical model of the BLDCM can be described as

$$\begin{cases} \frac{dy}{dt} = k_y\omega \\ \frac{d\omega}{dt} = \frac{k_t I}{J} - \frac{F_f}{J} - \frac{F_l}{J} \\ \frac{dI}{dt} = -\frac{RI}{L} - \frac{k_e\omega}{L} + \frac{k_u\rho}{L} \end{cases} \tag{1}$$

where y and ω are the angular position and velocity, respectively; I, L, and R denote the current, inductance, and the resistance of the armature, respectively; J is the rotor inertia; F_f and F_l are the friction and load torque, respectively; ρ represents the pulse width modulation (PWM) input to the motor; k_y, k_t, k_e, and k_u are the reduction ratio, torque constant, back electromotive force constant, and the input gain of the PWM, respectively. The precise modeling of the friction force F_f is rather difficult, while it is commonly accepted that the friction can be expressed as a static nonlinear function of the velocity and its dominant components include the Coulomb friction, stiction, Stribeck friction, and the viscous friction (Armstrong et al. (2001)).

3. ESO BASED SWITCHING CONTROLLER DESIGN

To achieve the aforementioned control objective, ADRC is designed first to compensate the friction as well as the motor parameter uncertainties and unmodeled dynamics. The motor dynamics in (1) can be reformulated as

$$\begin{cases} \dot{y}_1 = y_2 \\ \dot{y}_2 = y_3 \\ \dot{y}_3 = ay_2 + by_3 - c_1\left(F_f + F_l\right) - c_2\left(\dot{F}_f + \dot{F}_l\right) + K\rho \end{cases} \tag{2}$$

where

$$\begin{array}{l} y_1 = y,\ y_2 = k_y\omega,\ y_3 = k_y\dot{\omega},\ a = -\frac{k_t k_e}{JL},\ b = -\frac{R}{L}, \\ c_1 = \frac{k_y R}{JL},\ c_2 = \frac{k_y}{J},\ K = \frac{k_y k_t k_u}{JL} \end{array} \tag{3}$$

Note that $\dot{F}_f$ does not exist at the velocity reversal but it is not required for the controller design. Since the qualities of the calculated velocity and acceleration signals are really poor, the nominal dynamics $ay_2 + by_3$ in (2) cannot be compensated in a feedforward way but is regarded as the unknown disturbance. The total disturbance is defined as

$$f = ay_2 + by_3 - c_1\left(F_f + F_l\right) - c_2\left(\dot{F}_f + \dot{F}_l\right) \tag{4}$$

To eliminate the effect of f and reduce the phase lag, the following reduced-order ESO (RESO) is designed to provide the disturbance estimation

$$\begin{cases} \dot{w}_1 = -\beta_1 w_1 + w_2 + \left(\beta_2 - {\beta_1}^2\right) y_1 \\ \dot{w}_2 = -\beta_2 w_1 + w_3 + K\rho + \left(\beta_3 - \beta_1\beta_2\right) y_1 \\ \dot{w}_3 = -\beta_3 w_1 - \beta_1\beta_3 y_1 \end{cases} \tag{5}$$

where β_i $(i = 1, 2, 3)$ is the observer gain and can be determined by allocating all the poles at $-\omega_o$ (Gao (2003)), and w_i is the intermediate variable. The estimations of the velocity, acceleration, and total disturbance, z_1, z_2, and z_3 are in the form of

$$\begin{cases} z_1 = w_1 + \beta_1 y_1 \\ z_2 = w_2 + \beta_2 y_1 \\ z_3 = w_3 + \beta_3 y_1 \end{cases} \tag{6}$$

Taking the Laplace transformations of (5) and (6) yields

$$z_3 = \frac{{\omega_o}^3}{\left(s + \omega_o\right)^3} f \tag{7}$$

It can be seen that the disturbance estimation is the filtered value of the true disturbance. Combined with the PD control, the control law can be established as

$$\rho = k_p(y_r - y_1) - k_d\dot{y}_1 - z_3 \Big/ K \tag{8}$$

where y_r is the position command, and k_p and k_d are the proportional and derivative gains, respectively. Substituting (7) into (8) one can derive the two-degree-of-freedom expression of the control law as

$$\rho = \underbrace{\left(k_p + \frac{k_p\omega_o F}{3}\cdot\frac{1}{s}\right)}_{\rho_1} e - \underbrace{\left(\frac{k_d\omega_o F}{3} + k_d s + \frac{\omega_o F}{3K}s^2\right)}_{\rho_2} y_1 \quad (9)$$

where $e = y_r - y_1$, and $F = 3{\omega_o}^2/(s^2 + 3\omega_o s + 3{\omega_o}^2)$ is a low-pass filter. It can be seen that one degree of the controller is a PI-type control law ρ_1, and the other degree is a state feedback control law ρ_2. This kind of control structure can well solve the conflict between the tracking and disturbance rejection performances that is intrinsic in the conventional PID control. The value of ω_o affects the bandwidth of the low-pass filter, the gain of the integral effect which can eliminate the tracking error and also the gains of the state feedback which can provide the damping. Since the control law contains the integral action $[k_p\omega_o F/(3s)]e$, the undesirable limit cycle is prone to occur at low velocities.

When the Coulomb+static friction model is valid, there is no combination of PID parameters that can eliminate the limit cycle. This result makes clear why nonlinear modifications to the PID control are always necessary in practice (Armstrong and Amin (1996)). Inspired by the thought of designing nonlinear or logical integral control (Armstrong et al. (1994)), a switching strategy is proposed based on the above designed nominal controller to suppress the limit cycle. The idea originates from the cause of the limit cycle in the presence of the integral action. Fig. 1 is a rough representation of the generation process of the limit cycle. When the motor is in the stick state, the absolute value of z_3 keeps increasing until the control force overcomes the maximum stiction. Since the maximum stiction is larger than the Coulomb friction, the sliding motion with a large acceleration is initiated then, and z_3 begins to decrease at the same time. As the position approaches the command, z_3 is expected to provide a deceleration to attenuate the overshoot. While it can be seen that the polarity change of z_3 happens at the time later than that of desire due to the observation lag of the ESO. As the decrease of the control force and the increase of the friction force, the motor starts to decelerate and finally stops in a next stick. The alternation between the stick and slip is aroused thus. Considering the adverse effect of the ESO near the command, a switching control law is proposed as

$$\rho = k_p e - k_d\dot{y}_1 - \left[1 - \sigma\left(e, \dot{y}_r\right)\right] z_3 \Big/ K \quad (10)$$

where

$$\sigma\left(e, \dot{y}_r\right) = \begin{cases} 1, & L(e) = 0 \text{ and } |\dot{y}_r| < v_\delta \\ 0, & \text{else} \end{cases} \quad (11)$$

v_δ is the threshold of the low velocity below which the effect of the friction force is dominant. For the sake of brevity, the control signals for $\sigma\left(e, \dot{y}_r\right) = 1$ and $\sigma\left(e, \dot{y}_r\right) = 0$ are denoted as ρ_l and ρ_h, respectively. $L(e)$ is a hysteresis function

$$L\left(e\right) = \begin{cases} 1, & |e| > e_h \\ 0, & |e| < e_l \\ L_{-1}\left(e\right), & \text{else} \end{cases} \quad (12)$$

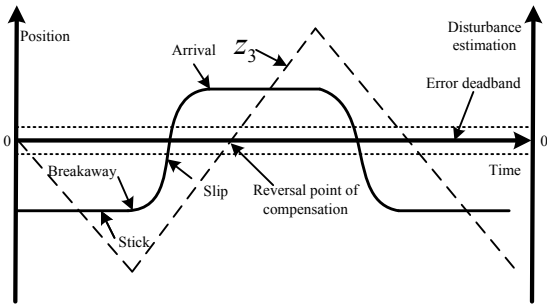

Fig. 1. Profile of the generation of the limit cycle.

where e_h and e_l are the switch-on and switch-off values, respectively, and $L_{-1}\left(e\right)$ denotes the function value at the last sampling time. The hysteresis function is employed to reduce the effect of the measurement noise on the switching strategy.

The thought behind (11) is quite simple that, when the motor operates within the low-velocity region and the precision requirement is satisfied, the disturbance estimation is abandoned in the control signal to avoid the unnecessary oscillation. The disturbance estimation is employed to reduce the tracking error when the command velocity is high or the tracking error is beyond the deadzone. When the motor enters the precision deadzone from a sliding motion, the switching from ρ_h to ρ_l is activated and the acceleration with only the PD control becomes much smaller than that with the compensation of z_3. Thus, the overshoot can be attenuated. The ideal case is that the velocity decreases to zero and the position just stops in the deadzone. Whether the ideal case can happen or not is determined by many factors like the control parameters and also the width of the deadzone. The system with larger PD control gains and a wider deadzone is more likely to achieve this. A similar approach employed in the integral control is resetting the integral term when the motion is detected or during the velocity reversals (Armstrong et al. (1994)).

4. LIMIT CYCLE ANALYSIS

In this section, the effect of the ADRC parameters on the limit cycle is investigated based on the describing function method. It is important to note that the describing function is an effective approach in predicting the limit cycle without the sticking when only the Coulomb friction is considered (Armstrong et al. (1994); Henrik and Astrom (2001)). For the case of Coulomb+stiction, the describing function method is not precise since there exists sticking in the resulted limit cycle and the zero velocity maintains not at isolated time instants but for a finite time interval. Only the Coulomb and Stribeck frictions are accounted for and the limit cycle without the sticking is the main concern of this section. The Coulomb and Stribeck frictions can be modeled as (Canudas de Wit et al. (1989))

$$F_f^{sc} = \begin{cases} F_f^s \text{sign}\left(\omega\right) + \frac{F_f^c - F_f^s}{\tau}\omega, & |\omega| \le \tau \\ F_f^c \text{sign}\left(\omega\right), & |\omega| > \tau \end{cases} \quad (13)$$

where F_f^c, F_f^s, and τ denote the Coulomb friction, the maximum stiction, and the Stribeck velocity, respectively.

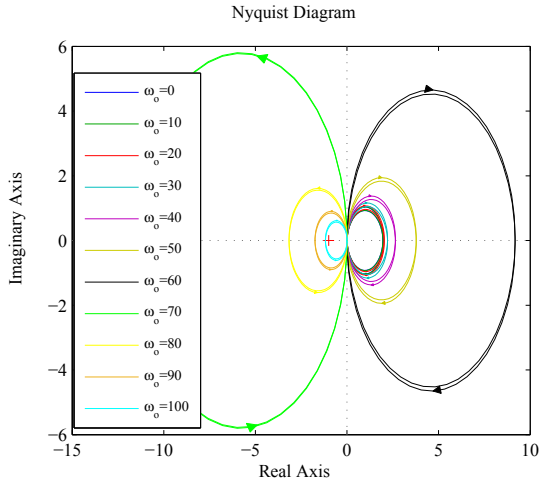

Fig. 2. Nyquist diagrams for different values of ω_o ($k_p = 50$, $k_d = 0.5$).

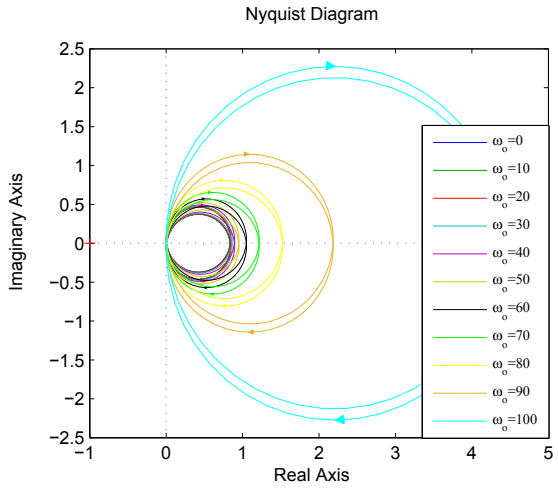

Fig. 3. Nyquist diagrams for different values of ω_o ($k_p = 50$, $k_d = 1.0$).

Denoting $N(A)$ as the describing function of F_f^{sc} can obtain

$$N(A) = \begin{cases} \frac{4}{\pi A} + \frac{F_f^c - F_f^s}{\tau}, & A \le \tau \\ \frac{4F_f^s}{\pi A} + \frac{2\left(F_f^c - F_f^s\right)\sin^{-1}(\tau/A)}{\tau\pi} + \\ \frac{2\left(F_f^c - F_f^s\right)}{\pi A}\sqrt{1 - \frac{\tau^2}{A^2}}, & A > \tau \end{cases} \tag{14}$$

The derivative of $N(A)$ with respect to the amplitude can be obtained as

$$N'(A) = \begin{cases} -\frac{4}{\pi A^2}, & A \le \tau \\ \frac{2\pi A\left[2\sqrt{A^2-\pi^2}\left(\left(F_f^s - F_f^c\right)\sqrt{A^2-\pi^2} - F_f^s A\right)\right]}{\pi^2 A^4 \sqrt{A^2-\pi^2}}, & A > \tau \end{cases} \tag{15}$$

Evidently, $N'(A) < 0$ holds. After obtaining $N(A)$, the open-loop dynamics of the BLDCM can be written as

$$G = \frac{k_t k_u k_y}{D_1 + N(A) D_2} \tag{16}$$

where $D_1 = JLs^3 + (JR + v_c k_y L)s^2 + (k_t k_e + v_c k_y R)s + k_l k_y L s + k_l k_y R$, $D_2 = k_y(Ls + R)s$, and v_c is the viscous friction coefficient. Making the denominator of the closed-loop transfer function be zero yields

Table 1. Critical parameter combinations of (ω_o, k_d) that do not generate the limit cycle.

ω_o	10	20	30	40	50	60	70	80	90	100
k_d	0.36	0.37	0.38	0.40	0.43	0.47	0.52	0.61	0.71	0.85

$$\frac{-1}{N(A)} = \frac{D_2}{D_1 + k_t k_u k_y (K_1 + K_2)} \tag{17}$$

where $K_1 = k_p + k_p \omega_o F/(3s)$, $K_2 = k_d \omega_o F/3 + k_d s + \omega_o F s^2/(3K)$. It is obvious that $-1/N(A) \to 0$ when $A \to 0$. The condition of no limit cycle is that the Nyquist plot does not intersect with the negative real axis.

Among the ADRC parameters, the proportional gain k_p determines the response speed directly, and it can be designed according to the criteria that the maximum control effectiveness can be utilized when the position error is larger than a specified value. K can be calculated based on the nominal model. Since ω_o is the cause of the limit cycle and k_d can provide the damping effect to suppress the limit cycle, the effects of these two parameters are investigated in the subsequent analysis. The nominal parameters of the BLDCM are

$$\begin{array}{l} J = \ 0.00005 \text{ kg} \cdot \text{m}^2, \ R = 0.36\ \Omega, \ L = 2.8 \text{ mH}, \\ k_y = \ 1/280, \ k_t = 0.19 \text{ N} \cdot \text{m/A}, \ k_e = 0.024\ V \cdot s/^\circ, \\ k_u = \ 100 \ \text{ V}, \ k_l = 0.5 \ \text{ N} \cdot \text{m}/^\circ, \ v_c = 0.1, \\ F_f^c = 0.48 \ \text{ V}, \ F_f^s = 0.74 \ \text{ V} \end{array} \tag{18}$$

The Nyquist plots for different values of ω_o with ($k_p = 50$, $k_d = 0.5$) and ($k_p = 50$, $k_d = 1.0$) are shown in Fig. 2 and Fig. 3, respectively. According to Fig. 2, it can be seen that the limit cycle is induced when ω_o exceeds a certain value. Similar result can be found in the PID control that a large integral gain tends to generate the limit cycle (Townsend and J. Kenneth Salisbury (1987)). k_d has to be increased to provide an adequate damping and eliminate the limit cycle as presented in Fig. 3. The critical parameter combinations (ω_o, k_d) that do not generate the limit cycle are shown in Table 1. As can be observed, there exists a monotonically increasing relationship between ω_o and k_d, which suggests that a large value of k_d has to be designed when ω_o is high. Consequently, the selection of ω_o is restricted when the SNR of the velocity is low and the available k_d is limited due to the noise. Since the conflict between the desired friction compensation capability and elimination of limit cycle cannot be solved in the conventional scheme, the switching strategy is proposed in this paper to improve the upper bound of ω_o.

5. EXPERIMENTAL RESULTS

In this section, experiments are performed to validate the effectiveness of the proposed method. For the sake of brevity, the algorithms with and without the switching strategy are called ADRC$_s$ and ADRC, respectively. The experimental setup is shown in Fig. 4. The processor employed is ARM STM32F427. The proposed algorithm was coded in C and the sampling period is 0.25 ms. The position signal is measured by a potentiometric displacement transducer and a second-order digital low-pass filter is used to filter the measurement. The velocity signal is obtained by the numerical differentiation. The specified

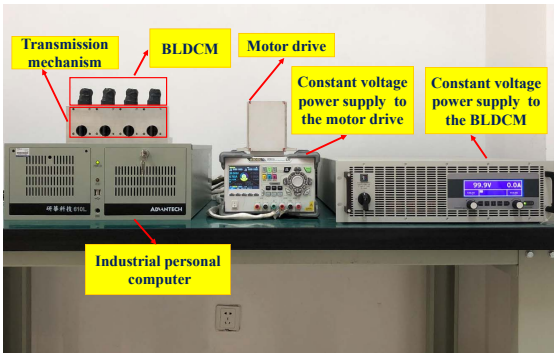

Fig. 4. Setup of the experimental system.

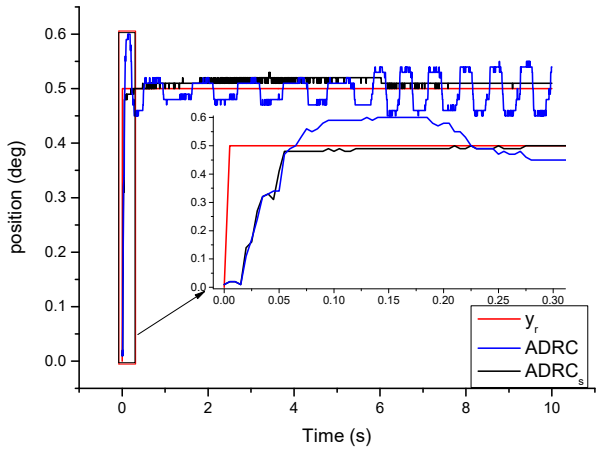

Fig. 5. Experiment result of the step response.

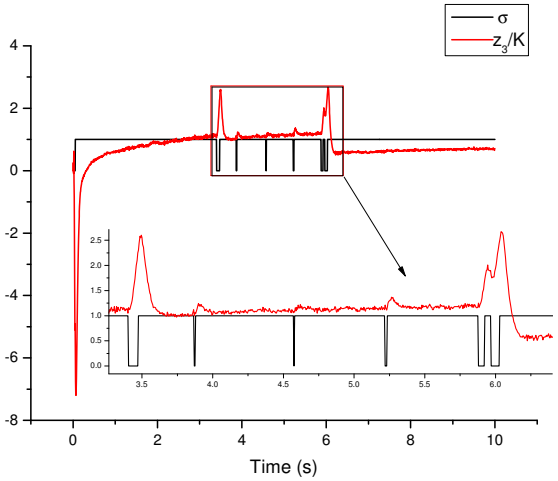

Fig. 6. Experiment results of the disturbance estimation and switching signal for ADRC_s.

settling time is less than 60 ms for a 1° position command. The filtered magnitude of the position noise is less than 0.02°. Considering the tracking precision and the switching frequency simultaneously, $e_l = 0.02$ and $e_h = 0.03$ are specified. $k_p = 50$, $k_d = 0.5$, and $\omega_o = 50$ are selected to achieve the desired tracking performance.

The experimental results for the step response are presented in Fig. 5 and Fig. 6. According to Table 1, there should be no limit cycle since the critical value for k_d is 0.43. However, the limit cycle can still be observed in the step response of ADRC. This can be interpreted by the fact that the stiction is neglected in the describing function analysis and thus a larger k_d is needed. After adding the switching strategy, the position stops at the first arrival of the deadzone. Both the limit cycle and the overshoot are eliminated and the transient performance is satisfactory. Since the position stops near the boundary of the deadzone in the beginning, there exist several switches in the steady state due to the noise disturbance as shown in Fig. 6. At the sixth second, there is a minor motion towards the command and the actual error becomes less than 0.01. Then, the motor stops completely since the magnitude of the filtered noise is less than 0.02 and the threshold for the next switching is 0.03.

When tracking the ramp command, it is known that the limit cycle happens only when the ramp rate is sufficiently low (Shen and Wang (1964)). The switching logic is unnecessary and may even degrade the tracking performance for the high-velocity case. Through conducting the experiments of tracking ramp commands with different rates, the velocity threshold v_δ can be determined by finding the critical velocity above which the advantage of the switching strategy disappears. Five ramp rates, $0.01°/s$, $0.02°/s$, $0.03°/s$, $0.04°/s$, and $0.05°/s$, respectively, are designed and the experimental results are given in Fig. 7 and Fig. 8. The standard deviations of the tracking errors for these five commands under ADRC are 0.031°, 0.018°, 0.011°, 0.013°, and 0.017°, respectively. For ADRC_s, the corresponding errors are 0.024°, 0.026°, 0.025°, 0.028°, and 0.028°, respectively. It can be seen that ADRC_s is more advantageous only for the extremely low velocities at which the oscillation exists. $v_\delta = 0.01$ can be selected for this BLDCM. The switching signal σ and z_3/K for $v_\delta = 0.01$ are presented in Fig. 8. Since the switching logic designed only depends on the error information whose precision is much higher, the switching frequency is acceptable.

6. CONCLUSION

In this paper, a friction-model free compensation approach was presented. The extended state observer was employed to estimate the friction and other disturbances. Since the observer can introduce the integral action, the limit cycle may be introduced. To eliminate the limit cycle under the restricted damping, a switching strategy was proposed to determine when the disturbance estimation should be added in the control signal. The switching strategy was enlightened by the fact that nonlinear modifications to the integral action is always necessary in the practical friction compensation. Hardware experiments were conducted to demonstrate the effectiveness of the proposed method.

REFERENCES

Ahmed-Ali, T., Romain, P., and Francoise, L.L. (2009). Continuousdiscrete adaptive observers for state affine systems. *Automatica*, 45(12), 2986–2990.

Armstrong, B. and Amin, B. (1996). PID control in the presence of static friction: A comparison of algebraic and describing function analysis. *Automatica*, 32(5), 679–692.

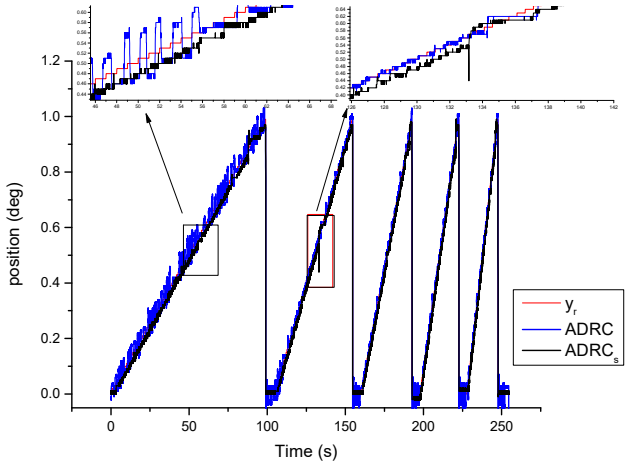

Fig. 7. Experiment result of the ramp response.

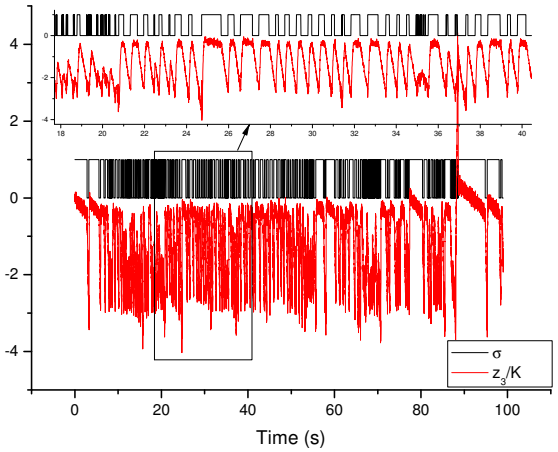

Fig. 8. Experiment results of the disturbance estimation and switching signal for $ADRC_s$.

Armstrong, B., Neevel, D., and Kusik, T. (2001). New results in NPID control: Tracking, integral control, friction compensation and experimental results. *IEEE Transactions on Control Systems Technology*, 9(2), 399–406.

Armstrong, B., Dupont, P., and Canudas de Wit, C. (1994). A survey of models, analysis tools and compensation methods for the control of machines with friction. *Automatica*, 30(7), 1083–1138.

Chen, W., Yang, J., Guo, L., and Li, S. (2016). Disturbance-observer based control and related methods -An overview. *IEEE Transactions on Industrial Electronics*, 63(2), 1083–1095.

Friedland, B. and Park, Y.J. (1997). Implementation of a friction estimation and compensation technique. *IEEE Control Systems*, 17(4), 71–76.

Gao, Z. (2003). Scaling and bandwidth-parameterization based controller tuning. In *Proceedings of the American Control Conference*, 4989–4996. Colorado, USA.

Garagić, D. and Srinivasan, K. (2004). Adaptive friction compensation for precision machine tool drive. *Control Engineering Practice*, 12(11), 1451–1464.

Han, J. (2009). From PID to active disturbance rejection control. *IEEE Transactions on Industrial Electronics*, 56(3), 900–906.

Henrik, O. and Astrom, K.J. (2001). Friction generated limit cycles. *IEEE Transactions on Control Systems Technology*, 9(4), 629–636.

Huang, S. and Tan, K.K. (2012). Intelligent friction modeling and compensation using neural network approximations. *IEEE Transactions on Industrial Electronics*, 59(8), 3342–3349.

Huang, W.S., Liu, C.W., Hsu, P.L., and Yeh, S.S. (2009). Precision control and compensation of servomotors and machine tools via the disturbance observer. *IEEE Transactions on Industrial Electronics*, 57(1), 420–429.

Ishikawa, J. and Tomizuka, M. (1998). Pivot friction compensation using an accelerometer and a disturbance observer for hard disk drives. *IEEE/ASME Transactions on Mechatronics*, 3(3), 194–201.

Jamaludin, Z., Brussel, H.V., and Swevers, J. (2009). Friction compensation of an XY feed table using friction-model-based feedforward and an inverse-model-based disturbance observer. *IEEE Transactions on Industrial Electronics*, 56(10), 3848–3853.

Lee, H.S. and Tomizuka, M. (1996). Robust motion controller design for high-accuracy positioning systems. *IEEE Transactions on Industrial Electronics*, 43(1), 48–55.

Canudas de Wit, C., Noel, P., Aubin, A., and Brogliato, B. (1989). Adaptive friction compensation in robot manipulators: low-velocities. *The International Journal of Robotics Research*, 10(3), 1352–1357.

Ren, C., Li, X., Yang, X., and Ma, S. (2019). Extended state observer-based sliding mode control of an omnidirectional mobile robot with friction compensation. *IEEE Transactions on Industrial Electronics*, 66(12), 9480–9489.

Shen, C.N. and Wang, H. (1964). Nonlinear compensation of a second- and third-order system with dry friction. *IEEE Transactions on Application and Industry*, 83(71), 128–136.

Sun, M., Wang, Z., Wang, Y., and Chen, Z. (2013). On low-velocity compensation of brushless DC servo in the absence of friction model. *IEEE Transactions on Industrial Electronics*, 60(9), 3897–3905.

Townsend, W.T. and J. Kenneth Salisbury, J. (1987). The effect of coulomb friction and stiction on force control. In *Proceedings of the IEEE International Conference on Robotics and Automation*, 883–889. Raleigh, USA.

Wang, L., Jiao, R., Li, Q., Yin, Y., and Zheng, Q. (2016). Active disturbance rejection control in stribeck friction dynamic compensation for high-accuracy servo systems. In *Proceedings of the Chinese Control Conference*, 4771–4775. Chengdu, China.

Xia, D., Wang, L., and Chai, T. (2013). Neural-network-friction compensation-based energy swing-up control of pendubot. *IEEE Transactions on Industrial Electronics*, 61(3), 1411–1423.